



The evaluation of electrical circuits for adjusting sound transmission properties of piezoelectric metamaterials

Guosheng Ji^a, Jie Zhou^{b,*}, John Huber^{a,*}

^a Department of Engineering Science, University of Oxford, Parks Road, Oxford, OX1 3PJ, UK

^b School of Aeronautics, Northwestern Polytechnical University, Xi'an, 710072, China

ARTICLE INFO

Communicated by S.D. Rosa

Keywords:

Acoustic metamaterials

Piezoelectric

External circuit

Transfer matrix

Transmission property

ABSTRACT

In rods and beams, piezoelectric patches with external circuits have been extensively studied to dampen structural vibrations at the sound source. This work uses a large flat-layer type of piezoelectric acoustic metamaterial (AM) model for noise attenuation in the sound transmission stage rather than at the sound source. This could be directly implemented as a large space sound transmission barrier at the interface of diverse media including gas, liquid, and solid materials. The general analytical model to derive acoustic properties of the piezoelectric acoustic metamaterial is established by the equivalent transfer matrix approach for normal incidence waves. This has been validated numerically using the finite element method and experimentally in the solid medium propagation for the first time. Moreover, a parametric study of sound transmission properties in air, water, and steel is conducted by adjusting external circuit parameters, flat-layer structures, and piezoelectric materials. The findings demonstrate the ability to control sound resonance frequency and bandwidth through the propagation process over a wide range using external circuit parameters alone. This endows the piezoelectric acoustic metamaterial with great versatility relative to conventional, fixed structure, metamaterials used as sound barriers at the interface of diverse media. In addition, the size of the piezoelectric AM can reach a deeply sub-wavelength level, less than 10^{-3} of the resonance wavelength in both water and solid media, which goes far beyond the wavelength-to-thickness ratio of classical acoustic metamaterials. The layer-type piezoelectric AM thus shows excellent performance in tunability and compactness for space-sensitive applications as well as great potential in combining metamaterials with electronic control.

1. Introduction

Noise pollution is a familiar nuisance in a wide variety of work and social situations, with structure-borne noise and air-borne noise [1] being the main types of acoustic disturbance. The high cost of noise pollution, both in terms of economic value and human health, has been recognized [2]. Similarly, high-frequency, structure-borne vibrations are recognized as a source of material fatigue and degradation [3]. Consequently, there is a drive to reduce both structure-borne and air-borne noise using interventions such as noise barriers and sound absorbers. Typical acoustic liners are layered composites including panels, honeycomb, porous or fibrous materials, and these are established in many applications. Meanwhile, the field of acoustic metamaterials (AMs) and metasurfaces has rapidly grown in recent years; these materials demonstrate anomalous properties, not found in conventional materials, and have been regarded as a breakthrough in the control of acoustic waves. Smith [4] defined a metamaterial as “a macroscopic composite

* Corresponding authors.

E-mail addresses: jiezhou@nwpu.edu.cn (J. Zhou), john.huber@eng.ox.ac.uk (J. Huber).

<https://doi.org/10.1016/j.ymssp.2023.110549>

Received 1 November 2022; Received in revised form 15 May 2023; Accepted 19 June 2023

Available online 7 July 2023

0888-3270/© 2023 The Author(s). Published by Elsevier Ltd. This is an open access article under the CC BY license (<http://creativecommons.org/licenses/by/4.0/>).

of periodic or non-periodic structures whose function is due to both its cellular architecture and chemical composition". For AMs, Shen's group [5] further defines the AMs based on their unique functions stating that "local resonance gave birth to exotic acoustic properties that were previously inconceivable. For example: negative effective mass density, negative effective bulk modulus." Ma [6] further explains that "the popular view at present is that the phononic crystals emphasize the periodicity of structures, while the acoustic metamaterials emphasize the negative effective parameters and subwavelength sizes of structure". From these ideas, metamaterials can be thought of as a kind of man-made materials achieving special properties that are not normally found, such as negative density or modulus. These AMs include local resonators and fibrous materials that interact with the acoustic energy at specific frequencies [7,8]. Various resonator types of AMs, including membrane and plate resonators, space-coiling structures, or Helmholtz resonators, have been explored [9].

AMs potentially enable many advances such as negative effective properties, enhanced sound absorption and insulation, extraordinary wave manipulation, acoustic wave focusing, and efficient energy harvesting [7,10–13]. Efforts are ongoing to develop AM-type acoustic liners with enhanced ability to suppress structure-borne noise and other sound wave manipulation functions. Excellent acoustic liner performance has been demonstrated over the desired frequency range, breaking the conventional mass law that normally links sound suppression directly to layer masses. For instance, exciting concepts have been proposed for sound absorbers and insulators combining improved acoustic performance and reduced size or weight relative to classical porous foams and Helmholtz resonators [14–20]. However, a challenge remains in the trade-off between effective bandwidth, efficiency, and device size. For instance, the thickness of current space-coiling, Helmholtz resonator, plate and membrane types of AMs is about 1/100 of the target resonance wavelength [21–25]. This significantly limits their applications in controlling low-frequency noise, where thicker and heavier acoustic liners are required. In addition, most AMs are passive structures with inherently narrow band gaps determined by structural resonance. Such AMs are not adaptable to changes in working conditions or environment: their characteristics remain constant, being in strict accordance with designed-in structural parameters. As a result, performance cannot be controlled or optimized in varying service conditions [8]. Finally, typical AMs, such as membrane resonators, require structural complexity that can result in fragility and a challenge for fabrication. Truly broad-bandwidth robust sound absorbers and insulators have yet to be achieved in practical devices.

Active piezoelectric AMs are a new type of device that offers the opportunity of extraordinary material properties with adjustable frequency range [8]. For instance, piezoelectric elements can be introduced into plate-type AMs to create electronic control and feedback mechanisms [26,27]. The dynamic densities or moduli of the AMs can then be modified, resulting in anomalous phenomena over variable and controllable frequency ranges. By incorporating active piezoelectric elements into plate-type AMs, improved sound absorption and transmission coefficients can be achieved over a wide and tunable frequency range [26,28,29]. This type of control is both conceptually simpler and more robust than other types of active AM control, including mechanical deformation [30–32], thermal expansion [33,34], and pressure control [34]. As a result, piezoelectric metamaterials shunted with adjustable external circuits might provide a way to overcome the shortcomings of existing acoustic metamaterials: thick acoustic liners, fixed working conditions, and so on. In addition, piezoelectric active AMs may be suitable for a very wide range of applications in acoustic engineering, such as the reduction of acoustic transmission in buildings, or the elimination of structure-borne vibration from machinery. Similarly, vibrations from railways, roads, marine systems and energy generation systems could also be alleviated.

On the side surfaces of rods and beams, piezoelectric patches shunted with external electrical circuits have been used to reduce mechanical vibrations [35,36]. By adding external electrical circuits, it was possible to modify the equivalent mechanical properties of piezoelectric patches and achieve a broad effective frequency range [37,38]. Due to pioneering work, piezoelectric patches with external electronic circuits have been extensively examined as a possible solution for damping structural vibrations and collecting mechanical energy from solid bar and beam systems [36,39–51]. A significant portion of structural vibration energy can be absorbed by inducing an external electrical resonance at the structure's resonance frequency. Adjustable resonant phenomena for mechanical vibration damping and energy harvesting have also been studied widely for solid rod [48,49] and beam [41,43–47,52,53] systems with attached piezoelectric patches.

In contrast, the investigation of transmission of an acoustic wave normally travelling through large flat piezoelectric metamaterials has made relatively little progress. In particular, the placement of piezoelectric metamaterials at the interface of diverse media, such as gas, liquid, and solid media needs investigation. The physical mechanism is distinct because flat piezoelectric metamaterials interact with and modify acoustic waves during sound propagation. To be more specific, the analysis of acoustic-structure interaction should take into account the coupling of two independent branches of physics, acoustics and structural mechanics. In some instances, the fluid's acoustic pressure and the solid's vibrations interact significantly [3]. Therefore, research on mechanical vibration damping by attaching piezoelectric patches to the side surfaces of rods and beams is not directly applicable to situations in which acoustic waves propagate through flat layers of a piezoelectric metamaterial [43,48,54,55].

Several analytical models have been developed to estimate sound wave transmission through periodic arrays of piezoelectric patches with external circuits, affixed to solid plates [26,28,29,40,50,54,55]. For instance, a semi-analytical model that predicts the acoustic properties of plate-type piezoelectric patches has been investigated using an equivalent electrical circuit model, taking electrical and mechanical properties into account [36,39]. However, obtaining the electrical impedance of piezoelectric patches still requires experimental data using an impedance analyser and piezoelectric resonance analysis software [39]. In addition, prior work does not account for structure-borne and airborne longitudinal waves with normal and oblique incidence angles [36,39]. The analytical models typically focus on a particular propagating medium, such as air or dense solids, rather than constructing a general model to predict transmission properties in all media [26,28,29,40,50,54,55]. Moreover, many of the mathematical models for piezoelectric patches have not been validated by experimental measurements [26,28,29,50].

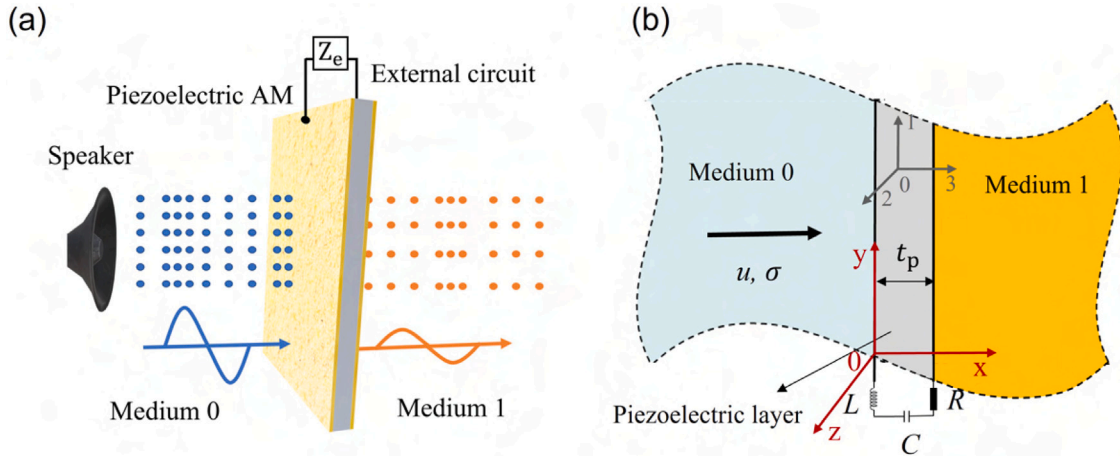


Fig. 1. (a) At the interface of two media, a typical acoustic wave impinges onto a piezoelectric layer shunted with an external circuit. (b) Schematic of acoustic waves propagating through a piezoelectric layer with an infinite lateral extent and uniform thickness while being switched by an external LCR circuit for analytical study.

The present work adds to the existing knowledge base by developing an analytical model using the transfer matrix approach to analyse the sound transmission property of a general layer-type piezoelectric AM with an external electrical circuit. The concept is applicable to varied propagation media, including gas, liquid, and solid materials. The piezoelectric AM is regarded as an equivalent isotropic layer, which is positioned at the interface of two media. The acoustic properties are directly derived using the moduli of elastic, piezoelectric, and dielectric permittivity of the piezoelectric material. One of the novelties in our research is to achieve anomalous acoustic performance by using a frequency-dependent elastic modulus. The frequency-dependent elastic modulus can be manipulated to negative values by adjusting external electrical circuits. We examine piezoelectric and acoustoelectric interactions for manipulating acoustic waves at normal incidence angles. It is found that the thickness of the piezoelectric AM may reach a sub-wavelength level, less than 10^{-3} of the resonance wavelength, surpassing the wavelength-to-thickness ratio (about 10^{-2} of the resonance wavelength) for other AMs [21–25]. A systematic study of attenuating longitudinal sound waves in a variety of media is undertaken. This includes fundamental mechanisms, experimental validation, and parametric investigation [26,28,29,50]. This work thus expands the applicability of the analytical model from a single medium to many media and provides experimental validation [26,28,29,40,50,54,55]. Finally, the piezoelectric AM demonstrates great versatility relative to conventional, fixed structure metamaterials. The opportunities and challenges associated with applying piezoelectric AMs to practical sound adsorption tasks are identified, along with methods for optimizing device performance. The analytical model also demonstrates a potential to build connections with classical acoustic liners, such as porous foams, Helmholtz resonators, and perforated panels. It indicates a new research direction to combine piezoelectric AMs with classical acoustic liners for further improvement in noise reduction.

2. Acoustic response for normal incidence

A layered piezoelectric AM is studied in Fig. 1(a), with an infinite lateral extent and uniform thickness. The piezoelectric layer is coated with thin conductive electrodes whose mechanical impedance is taken to be negligible, and that is assumed to be well insulated from conductive media. Transfer matrices for the layers are next developed and combined to give the transfer matrix for the piezoelectric AM.

2.1. Transfer matrix of a piezoelectric layer

A piezoelectric layer of density ρ_p with its local 3-axis aligned to the x -direction is shown in Fig. 1(b), sandwiched by semi-infinite environment media. An active external circuit, with an electrical impedance Z_e , is connected across the piezoelectric layer using an electrode pair. For example, Z_e could comprise series resistance R , inductance L and capacitance C . The piezoelectric layer is modelled subject to one-dimensional longitudinal wave propagation at normal incidence angle, neglecting any transverse and shear effects [56]. Then all stress and electric displacement components other than stress σ_3 and electric displacement D_3 are negligible. The relevant constitutive relations (see Supplementary for another complicated derivation) reduce to

$$\begin{bmatrix} \sigma_3 \\ D_3 \end{bmatrix} = \begin{bmatrix} c_{33}^E & e_{33} \\ e_{33}^S & -\epsilon_{33}^S \end{bmatrix} \begin{bmatrix} \frac{\partial u}{\partial x} \\ \frac{\partial \psi}{\partial x} \end{bmatrix}, \quad (1)$$

where u is through-thickness displacement, and ψ is the electric potential. The superscript S denotes that the respective coefficient is evaluated at constant strain, and superscript E indicates a constant electric field. c^E , e , and e^S are complex elastic constant, piezoelectric stress constant and dielectric permittivity, respectively.

The component values in the external circuit can be modified to control the resonance frequency and degree of damping. The corresponding circuit equation is [26]

$$IZ_e = \psi_r - \psi_l, \quad (2)$$

where I is the current in the external circuit, while ψ_r and ψ_l are electric potentials on the right and left surfaces of the piezoelectric layer in Fig. 1(b), respectively. The external circuit's phasor current at frequency ω can be given as $I = i\omega AD_{3l} = i\omega AD_{3r} = i\omega AD_3$, where A is the cross-sectional area of the piezoelectric layer. From Eq. (2), the electric displacement is $D_3 = D_{3l} = D_{3r} = \frac{1}{-i\omega AZ_e}(\psi_l - \psi_r)$. The transfer matrix \mathbf{T}_p of the sound wave propagating through a piezoelectric layer with an external circuit can be obtained. This relates the complex amplitude U of the displacement u and the amplitude S of the pressure σ on the two surfaces of the piezoelectric layer as (see the full derivation in the supplementary):

$$\begin{bmatrix} U_r \\ S_r \end{bmatrix} = \mathbf{T}_p \begin{bmatrix} U_l \\ S_l \end{bmatrix}, \quad (3)$$

where

$$\left\{ \begin{array}{l} \mathbf{T}_p(1, 1) = \cos(k_p t_p) - \frac{\sin(k_p t_p)(\cos(k_p t_p) - 1)}{\frac{e_{33}^S}{e_{33}^E} t_p (-i\omega Z_e C_0^S - 1)\omega z_p + \sin(k_p t_p)} \\ \mathbf{T}_p(1, 2) = \frac{1}{\omega z_p} \left(\sin(k_p t_p) - \frac{\sin^2(k_p t_p)}{\frac{e_{33}^S}{e_{33}^E} t_p (-i\omega Z_e C_0^S - 1)\omega z_p + \sin(k_p t_p)} \right) \\ \mathbf{T}_p(2, 1) = -\omega z_p \left(\sin(k_p t_p) - \frac{(\cos(k_p t_p) - 1)^2}{\frac{e_{33}^S}{e_{33}^E} t_p (-i\omega Z_e C_0^S - 1)\omega z_p + \sin(k_p t_p)} \right) \\ \mathbf{T}_p(2, 2) = \cos(k_p t_p) - \frac{\sin(k_p t_p)(\cos(k_p t_p) - 1)}{\frac{e_{33}^S}{e_{33}^E} t_p (-i\omega Z_e C_0^S - 1)\omega z_p + \sin(k_p t_p)} \end{array} \right. \quad (4)$$

$C_0^S = e_{33}^S A / t_p$ is the internal capacitance of the piezoelectric layer at constant strain. t_p is the piezoelectric layer thickness. $k_p = \omega / c_p$ is the wavenumber, and $z_p = \rho_p c_p$ is the characteristic impedance of the piezoelectric layer, with $c_p = \sqrt{\frac{e_{33}^E + e_{33}^2 / e_{33}^S}{\rho_p}}$ being the sound speed in the piezoelectric material. The whole piezoelectric layer can be treated as a unit cell, which can be further extended to a repeated structure.

2.2. Acoustic properties of piezoelectric AMs

In order to obtain the sound transmission and reflection coefficients, a scattering matrix \mathbf{H} can be derived (see supplementary for details),

$$\begin{bmatrix} U_r^+ \\ U_l^- \end{bmatrix} = \mathbf{H} \begin{bmatrix} U_l^+ \\ U_r^- \end{bmatrix} = \begin{bmatrix} \mathbf{T}'(1, 1) - \frac{\mathbf{T}'(1, 2)\mathbf{T}'(2, 1)}{\mathbf{T}'(2, 2)} & \frac{\mathbf{T}'(1, 2)}{\mathbf{T}'(2, 2)} \\ -\frac{\mathbf{T}'(2, 1)}{\mathbf{T}'(2, 2)} & \frac{1}{\mathbf{T}'(2, 2)} \end{bmatrix} \begin{bmatrix} U_l^+ \\ U_r^- \end{bmatrix}, \quad (5)$$

where

$$\mathbf{T}' = \begin{bmatrix} \exp(ik_0 N t_u) & 0 \\ 0 & \exp(-ik_0 N t_u) \end{bmatrix} \begin{bmatrix} 1 & 1 \\ -i\omega z_1 & i\omega z_1 \end{bmatrix}^{-1} \mathbf{T} \begin{bmatrix} 1 & 1 \\ -i\omega z_0 & i\omega z_0 \end{bmatrix}. \quad (6)$$

The superscripts + and - refer to forward propagating (+x) wave components and backward (-x) propagating wave components respectively. In environment medium 0, k_0 is the wavenumber, $z_0 = \rho_0 c_0$ is the characteristic impedance, ρ_0 is the density, and $c_0 = \sqrt{Y_0 / \rho_0}$ is the longitudinal wave speed. Correspondingly, in medium 1, the values are k_1 , ρ_1 , $z_1 = \rho_1 c_1$, and $c_1 = \sqrt{Y_1 / \rho_1}$. Y is the elastic modulus of the non-piezoelectric material. For multiple layers, the total transfer matrix \mathbf{T} is $\mathbf{T} = (\mathbf{T}_n \mathbf{T}_p)^N$, where N is the number of the bilayer. $t_u = t_n + t_p$ is the bilayer's thickness. Then, the sound pressure amplitude reflection coefficient r_a^+ and transmission coefficient t_a^+ , and sound energy absorption coefficient a_a^+ for longitudinal waves impinging into the active piezoelectric AM in the positive direction can be expressed as [57],

$$\left\{ \begin{array}{l} r_a^+ = |\mathbf{H}(1, 2)| \\ t_a^+ = |\mathbf{H}(1, 1)| \\ a_a^+ = 1 - (r_a^+)^2 - (t_a^+)^2 \end{array} \right. \quad (7)$$

Accordingly, the sound transmission loss is defined as,

$$\text{STL} = -20 \log t_a^+. \quad (8)$$

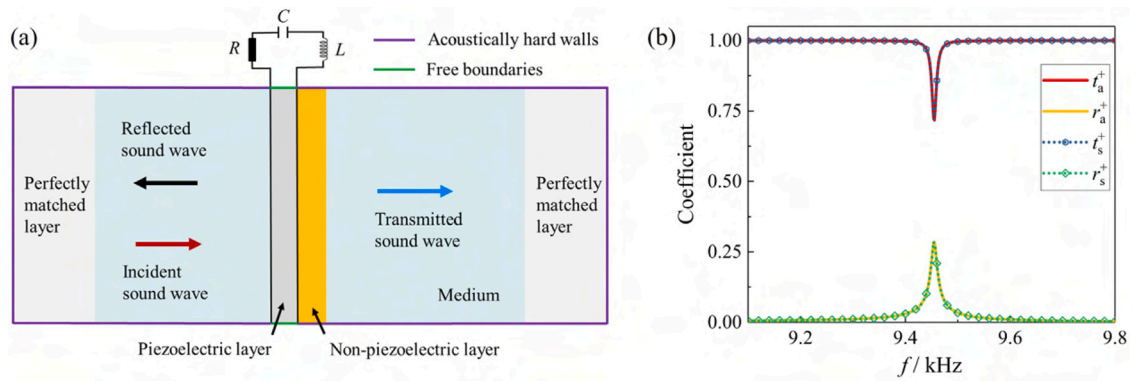


Fig. 2. (a) Cross-sectional view of a three-dimensional numerical simulation setup for obtaining sound transmission and reflection coefficients with perfectly matched layers adopted at sound wave entry and exit boundaries to avoid reflection waves from boundaries. (b) Transmission and reflection coefficients of the bilayer obtained in both analytical study (r_a^+ and r_a^-) and numerical simulation (r_s^+ and r_s^-).

Table 1

Properties of piezoelectric, non-piezoelectric and medium materials.

Medium	ρ / kgm ⁻³	c_{33}^E / GPa	e_{33} / Cm ⁻²	e_{33}^S / Fm ⁻¹	Y / GPa
PZT-5H	7500	83	29	1.416×10^{-8}	
PVDF	1780	1.2	-0.161 [58]	6.726×10^{-11}	
Fibrous PVDF	170 [59–61]	12×10^{-3} [59,60]	-8×10^{-5} [62–64]	1×10^{-11} [65]	
Copper	8500				100
Steel	7500				200
Water	997				2.1
Air	1.225				142×10^{-6}

3. Numerical and experimental validation for a normally incident sound wave

A three-dimensional numerical simulation is performed to validate the analytical estimates of acoustic properties of piezoelectric metamaterials by using the modified transfer matrix method. The transfer matrices of classical liners, including porous foams, Helmholtz resonators, isotropic membranes, and plates, have been well developed [56]. The modified transfer matrix method offers an opportunity to optimize multiple structures by combining piezoelectric AMs with classical acoustic liners. As a result, the current piezoelectric AM is set up as a bilayer structure with an additional copper layer. The acoustic pressure field of longitudinal waves propagating in the medium and non-piezoelectric layers is governed by the Helmholtz equation in a finite element solver COMSOL Multiphysics. However, the electromechanical behaviour of the piezoelectric layer shunted with an external circuit is governed by Newton's equation, the piezoelectric constitutive equation, and the circuit equation. For simplicity, we set medium 0 and medium 1 of Fig. 1 to be the same medium.

A sectional view of the arrangement of materials in a three-dimensional numerical simulation is given in Fig. 2(a). Plane waves are incident on the bilayer, where some sound energy is reflected into the original medium, and some are transmitted through the bilayer. The total transfer matrix of the bilayer is $\mathbf{T} = \mathbf{T}_n \mathbf{T}_p$, where \mathbf{T}_n is the transfer matrix of a non-piezoelectric layer. An external circuit, consisting of a resistor R , a capacitor C , and an inductor L in series, is connected across both sides of the piezoelectric layer to transfer electro-mechanical energy. As a result, the external electrical impedance is set as $Z_e(\omega) = R + i\omega L + 1/(i\omega C)$. The sound wave entry and exit boundaries of the computational domain are modelled using perfectly matched layers to avoid sound wave reflection. The whole three-dimensional computational domain is surrounded by two types of boundaries, as shown in Fig. 2(a). The side boundaries of the piezoelectric layer, consisting of in-plane and out-of-plane boundaries, are set as free boundaries without constraints. However, the side boundaries of the environmental medium, non-piezoelectric, and perfectly matched layers are acoustically hard walls. The maximum element size in the computational domain is smaller than one-fifth of the minimum target wavelength to ensure accurate simulations of wave dispersion properties.

A numerical validation case study was performed, where steel, PZT-5H and copper are assumed as the environmental medium, piezoelectric, and non-piezoelectric layers, respectively. Their properties are listed in Table 1. The thicknesses of the PZT-5H layer, t_p , and the non-piezoelectric copper layer, t_n , are 0.2 mm and 0.15 mm, respectively. The cross-sectional area A of the bilayer is 400 mm². For the external circuit, the parameters of the electronic components are set to arbitrary but readily obtainable values $R = 1 \Omega$, $C = 20 \text{ nF}$, and $L = 20 \text{ mH}$. As a result, the sound transmission and reflection coefficients obtained in the analytical study match well with the numerical study over the frequency domain, as shown in Fig. 2(b). This indicates the transfer matrix method's reliability in analysing the acoustic properties of both non-piezoelectric layers and piezoelectric layers with an external circuit for normally incident sound waves.

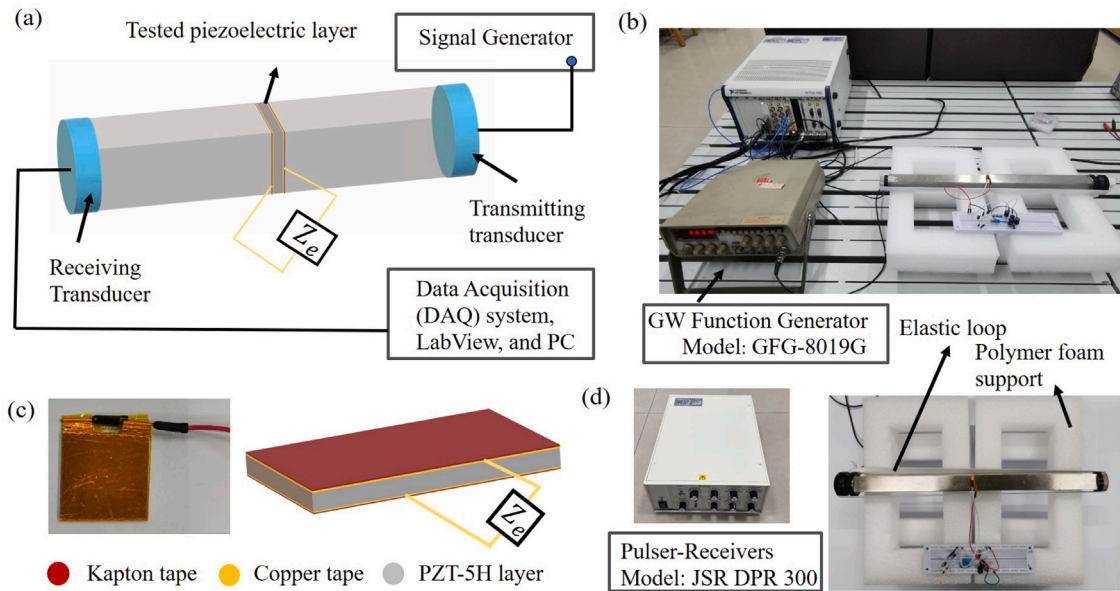


Fig. 3. (a) Schematic of a waveguide measuring system used to obtain experimental data. (b) The experimental system. (c) Multiple-layer structure of the PZT layer fabrication with an external circuit. (d) Using an ultrasonic pulser-receiver to introduce a broadband ultrasonic pulse into the steel waveguides to validate the reliability of experimental measurements, and a supporting system to eliminate environmental mechanical vibration.

A waveguide measurement rig was created to confirm the analytical and numerical findings, with Figs. 3(a-d) depicting the schematic, test facility, fabricated piezoelectric layer, and supporting structures respectively. The experimental setup comprised a pair of ultrasonic broadband transmitting/receiving transducers with a centre frequency of about 1 MHz and a diameter of 25 mm (Olympus Panametrics Ultrasonic Contact Transducer V102). A function generator (GW Function Generator GFG-8019G) produced an ultrasonic sinusoidal wave that was applied to the transmitting transducer, thus feeding longitudinal probing waves into the steel bar waveguide. Coupling gel (Olympus Panametrics Couplant B2) was used to eliminate acoustic impedance mismatch, and an elastic loop lightly clamped the acoustic components together. A foamed polymer support structure was used to minimize ultrasonic wave dispersion, see Fig. 3(d). The piezoelectric PZT-5H layer was placed between the steel input and output bars, of size $20\text{ cm} \times 2.5\text{ cm} \times 2.5\text{ cm}$, acting as waveguides. The receiving transducer collected the acoustic signal through the waveguide; this signal was sampled for 0.1 s and digitized using a National Instruments Data Acquisition System and high-speed digitizer (ART Technology with a sample rate of 40 MHz). Using the sinusoidal wave generator, tests were conducted from 20 kHz to 100 kHz. Afterwards, the data was post-processed to estimate the transmission spectrum. To provide a separate validation of these measurements, an ultrasonic pulser-receiver (model JSR DPR 300) was used to transmit a broadband ultrasonic pulse through the acoustic path. The resulting broadband data was processed using Fast Fourier Transforms to provide a frequency response spectrum.

As demonstrated in Fig. 3(c), the piezoelectric layer is constructed as a multilayer structure. A PZT-5H layer ($1\text{ mm} \times 2.5\text{ cm} \times 2.5\text{ cm}$), poled in its thickness direction, was coated with silver electrodes bonded to copper tape (Model 3M1181) flat conductive layers with a thickness of $66\text{ }\mu\text{m}$. These conductive electrodes were connected to the external series LCR circuit. To prevent electrical leakage to the steel bars, the whole piezoelectric sandwich was electrically isolated using $55\text{ }\mu\text{m}$ -thick Kapton tape (Beilong Electronics).

During experimental testing, the series LCR circuit using commercial electronic components had $L = 382.6\text{ }\mu\text{H}$, $C = 10.299\text{ }\mu\text{F}$ and $R = 4.296\text{ }\Omega$. The internal capacitance of the PZT-5H structure is $C_0^S = 9.210\text{ nF}$, measured using an LCR meter at 67 kHz (VICTOR 4082 handheld LCR meter). More generally, in the later parametric study, the range of inductance values considered might entail large components with significant resistance, making it impractical to build such a system from passive components. Instead, the external electrical circuits may be implemented electronically by utilizing digital signal processors like Arduino, Teensy, and Atmel [66]. For the sinusoidal wave generator, we can determine the voltage response and its associated amplitude over the frequency domain by converting the receiving transducer voltage signal from the time domain into the frequency domain using the fast Fourier transform. At the resonance frequency of the LCR circuit, the voltage amplitude of the receiving transducer is altered by switching the external circuit from open to closed. The ratio of transmitted voltage amplitude with closed and open circuit conditions indicates the effect of the external circuit. This ratio is shown in Fig. 4, labelled 'Exp. MP(GW)' indicating results from the GW GFG-8019G signal generator with multiple (MP) internal sound reflections included. Also shown is the result from the JSR DPR 300 broadband pulse generator, labelled 'Exp. MP(JSR)'. These results were computed by sampling 1.6 ms of the transmitted pulse with both open and closed circuit conditions. After fast Fourier transforming the received signals, the ratio of transmitted amplitude with and without the external circuit was computed at each frequency. There is reasonable agreement of the experimental data obtained from single frequency measurements (GW) and broadband measurements (JSR). However, it is noted that the presence of multiple

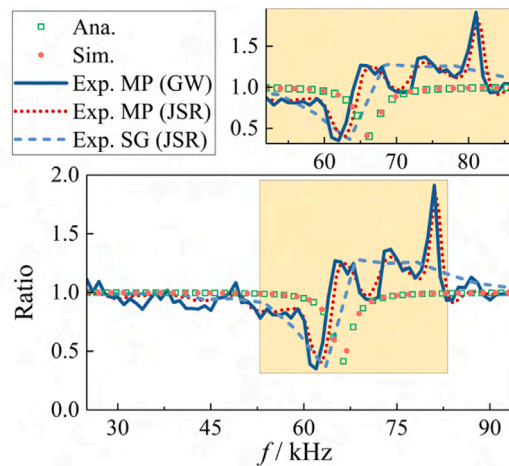


Fig. 4. The ratio of transmitted acoustic wave amplitude with closed and open circuit conditions obtained in the analysis ('Ana.') and simulation ('Sim.'). and the ratio of transmitted transducer voltage amplitude with closed and open circuit conditions, obtained from single frequency measurements (GW) and broadband measurements (JSR) in the presence of multiple reflections (MP) and single (SG) transmitted wave.

reflections (MP) in the experiment appears to generate a peak, at around 80 kHz, not seen in the analytical or simulation results. In order to simulate the experimental setup, it may be preferable to employ a sound soft boundary, which enforces a complete vanishing of total acoustic pressure at the boundary. However, for the specific case of transducers located at both ends of a solid bar containing complex structures and electronic components, sound soft boundaries are not sufficiently accurate to simulate the setup. Moreover, practical factors such as minor impedance mismatch between the steel bar and transducers, as well as the presence of coupling gel, present additional challenges in accurately determining the boundary conditions. To mitigate the influence of these factors and test whether this peak is indeed an artefact of reflected waves, the JSR test was repeated using a shorter time sample (0.16 ms), calculated to be short enough to prevent longitudinal wave reflections from influencing the results. In this scenario, a perfectly matched layer is more suitable for simulating the experimental tests. The resulting ratio of the open circuit to closed circuit amplitude is shown in Fig. 4, labelled 'SG (JSR)' to indicate a single (SG) transmitted wave. In this case the 80 kHz peak is suppressed, while the predicted dip in transmission around 60–70 kHz remains, giving improved agreement with the analytical calculations and numerical simulation. There remains some discrepancy between the models and experimental data, while the main feature, the attenuation in the 60–70 kHz range produced when the external resonant circuit is connected, is reproduced well. It can thus be concluded that external circuits can be used to modify the acoustic characteristics of a piezoelectric layer and this effect is captured with reasonable accuracy in the analytical model. Several potential causes could account for the frequency variation in experimental and simulation findings. First, analysis and numerical simulation ignore the anisotropic piezoelectric properties of the PZT layer by treating it homogeneously. These anisotropic characteristics could have minor effects on the resonance frequency. Second, analytical models frequently neglect the insignificant transverse and shear effects in the piezoelectric layer, which are subject to one-dimensional longitudinal wave propagation [56]. In experimental tests, however, a full set of elastic and piezoelectric properties, such as c_{13}^E , e_{11}^S and e_{31} , remains, leading to a frequency deviation. Thirdly, experimental measurements reveal the effects of Kapton tape, copper tape, and coupling gel that neither analytical models nor numerical simulations account for. This missing component might cause frequency dispersion as well as multiple sound reflections and interactions within the waveguide. Overall, while the transfer matrix method predicts the acoustic properties of piezoelectric AM with reasonable accuracy and minimal computational costs, its limitations highlight the need for future studies to account for the aforementioned factors. Validation of the model using air as a surrounding medium was attempted, but this proved challenging because even slight leakage can compromise the results. This issue potentially limits the applicability of layered sound absorbers in air if sound can bypass the absorber.

4. Acoustic performance of piezoelectric AMs in steel

The acoustic properties of a layered piezoelectric AM, such as sound transmission, reflection and absorption coefficients, are next studied analytically, using the transfer matrix method. A parametric study is performed based on a piezoelectric layer with various combinations of external circuit parameters L , C , R , layer thickness t_p , and multi-layer design. The relations among maximum sound absorption, transmission loss, and full width at half maximum (FWHM) are assessed to quantify acoustic performance and to identify trade-offs between absorption and bandwidth. The parametric study is conducted using steel as a typical external medium relevant to the suppression of structure-borne noise. However, a wide range of external media is possible, from dense solids to low-density fluids. This results in qualitative differences in performance due to the wide range of impedance mismatches. The electromechanical coupling of piezoelectric AMs can be maximized near the resonance frequency of the LC circuit. Far from this resonating frequency, the coupling is significantly weakened where the resonant frequency does not change with adjusting resistance R . It indicates an approach to improving the acoustic properties of piezoelectric AMs. With this in mind, the performance of the AMs in water and air is also briefly discussed.

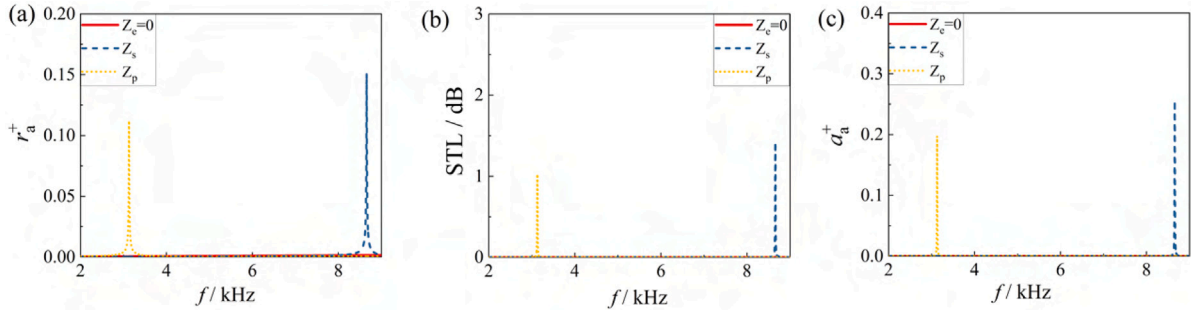


Fig. 5. Influence of the circuit type on (a) reflection coefficient, (b) transmission loss and (c) absorption coefficient.

4.1. Effects of the circuit type on acoustic properties

Taking steel as the external medium and a PZT-5H layer as the active component, the circuit configuration, or more precisely, the electrical impedance may directly affect the acoustic performance of piezoelectric AMs. The thickness of the PZT-5H layer t_p used in this study is 0.2 mm. The cross-sectional area A of the bilayer is 9 cm², while $R = 1 \Omega$, $C = 20$ nF and $L = 20$ mH are the electrical component parameters for the external circuit. Under short and open circuit conditions, only resonance effects near the mechanical resonance frequency of the piezoelectric layer should be expected. Resonance phenomena that are of interest in this study are caused mostly by the external circuit and not by mechanical resonance. Consequently, the effects of external circuits are investigated relative to a base case with a short circuit ($Z_c = 0$). On this premise, the acoustic performance of piezoelectric AMs is investigated in conjunction with two external electrical circuit conditions, including LCR circuits in series and parallel configurations (series RL // parallel C).

For series LCR external circuit, the equivalent electrical impedance Z_s is derived as,

$$Z_s = \frac{Z_c^s Z_0}{Z_0 + Z_c^s}, \quad (9)$$

where $Z_0 = 1/(i\omega C_0^S)$ and $Z_c^s = R + i\omega L + 1/(i\omega C)$. The resonant frequency corresponds to a frequency at which Z_s becomes purely real. Thus, it results in a large circulating current at resonance due to the energy oscillations. The electrical resonance frequency is

$$f_s = \frac{1}{2\pi} \sqrt{\frac{2C_0^S L + C(L - C_0^S R^2) + \sqrt{C(-4C_0^S L R^2 + C(L - C_0^S R^2)^2)}}{2C_0^S C L^2}}. \quad (10)$$

If $L \gg C_0^S R^2$ and $L \gg (C_0^S)^2 R^2 / C$, which is the case for most of our examples, the resonance frequency reduces to

$$f_s = \frac{1}{2\pi \sqrt{LC}} \sqrt{1 + \frac{C}{C_0^S}}, \quad (11)$$

which is independent of R . For the parallel LCR external circuit (RL // C), the equivalent electrical impedance becomes

$$Z_p = \frac{i\omega L + R}{1 + i\omega(C_0^S + C)(i\omega L + R)}, \quad (12)$$

and the corresponding electrical resonance frequency is

$$f_p = \frac{1}{2\pi \sqrt{L(C + C_0^S)}} \sqrt{1 - R^2 \frac{C + C_0^S}{L}}. \quad (13)$$

Frequencies f_s and f_p correspond approximately to resonances of the whole system, but do not exactly match the whole system resonance because they neglect the electro-mechanical coupling of the piezoelectric layer, treating it as a pure capacitance. As seen in Fig. 5, the presence of series or parallel LCR circuits results in resonant phenomena in which the sound transmission loss is greatly increased, and the external circuit dissipates a portion of the acoustic energy. However, the resonant phenomena produced by external circuits are not present in short-circuited piezoelectric layers. For simplification, the following sections focus primarily on the application of piezoelectric AMs with series LCR circuits in acoustic wave control.

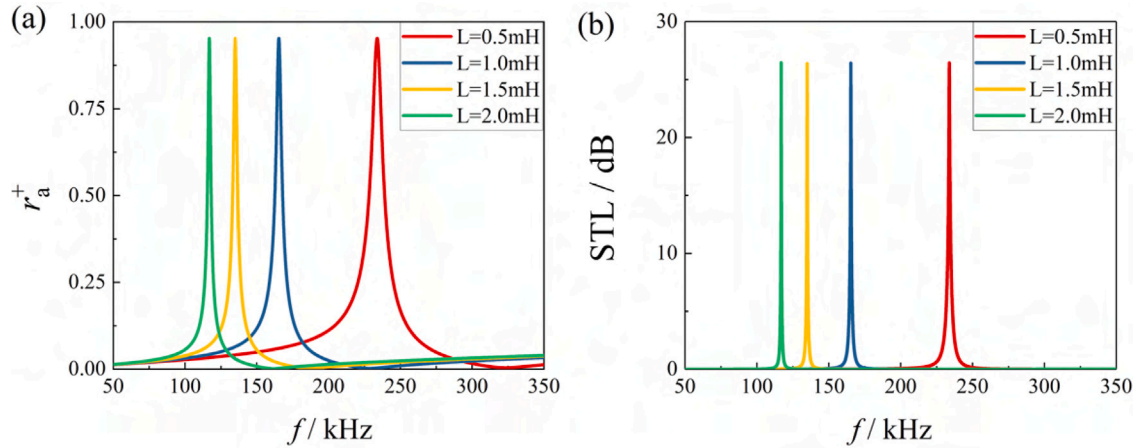
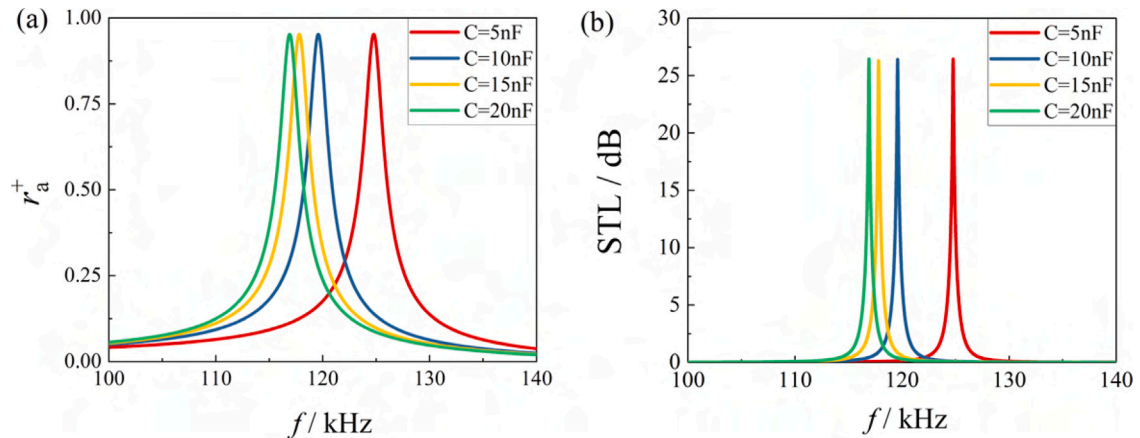
4.2. Effects of the circuit parameters on acoustic properties

The external circuit parameters can control both the electrical resonance frequency and bandwidth of the piezoelectric AM. Also, the internal capacitance C_0^S of the piezoelectric AM itself has a significant effect on the acoustic properties.

Table 2

Piezoelectric PZT-5H AMs tested in steel (—: not applicable; ×: variables).

Component	Property	T1	T2	T3	T4	T5	T6	T7
Variables		L	C	R	bilayer	R	t_p	t_p
Structure	t_p /mm	0.2	0.2	0.2	4	4	×	×
	t_n /mm	0.15	0.15	0.15	—	—	—	—
	A /mm ²	8	8	8	6400	6400	6400	2500
Circuit	C/nF	20	×	20	20	20	20	0.1
	L/mH	×	2	2	×	20k	20k	0.001
	R/Ω	1	1	×	10	×	10	0.001

**Fig. 6.** Influence of the external inductance L on (a) reflection coefficient and (b) transmission loss in T1 of Table 2.**Fig. 7.** Influence of the external capacitance C on (a) reflection coefficient and (b) transmission loss in T2 of Table 2.

As shown in Fig. 6, structure-borne noise is highly insulated by the piezoelectric AM at resonance. Additionally, the resonance frequency can readily be shifted: here variation between 230 kHz and 120 kHz is achieved by increasing inductance from 0.5 to 2 mH, making the AM adaptable to various frequencies. Realizing tunable resonance frequency is challenging when using passive AMs with fixed structure [67–69]. It is also evident that the bandwidth increases greatly as the external inductance is reduced. The results indicate that the resonance phenomenon can be controlled over a wide frequency range by adjusting the inductance in the external circuit. The external capacitance can play a similar role in adjusting the resonance frequency, as shown in Fig. 7. However, the external capacitance is less effective in manipulating resonance because of the constant series capacitance of the piezoelectric element itself. Note that variations of the external inductance and capacitance change the resonance frequency and bandwidth but do not affect the peak values of reflection coefficient and transmission loss.

Varying the external resistance indicates that it has no significant effect on the resonance frequency, see Fig. 8. However, the resonance sound reflection coefficient, transmission loss and absorption coefficient can be adjusted using the external resistance.

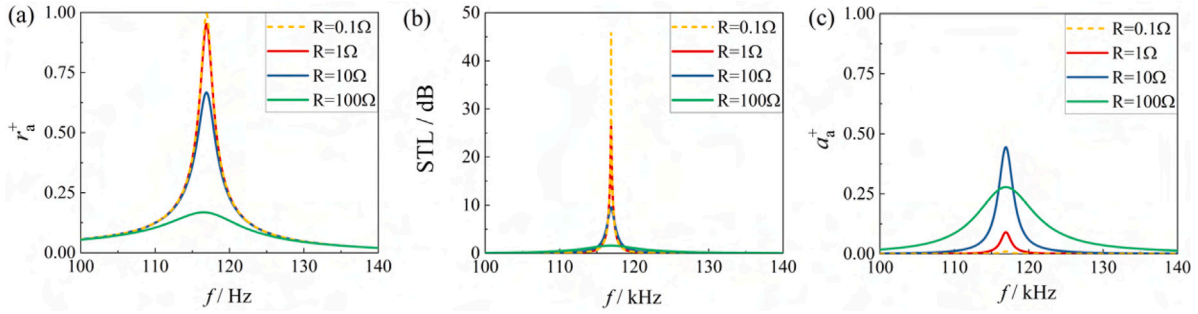


Fig. 8. Influence of the external resistance R on (a) reflection coefficient, (b) transmission loss, and (c) absorption coefficient in T3 of Table 2.

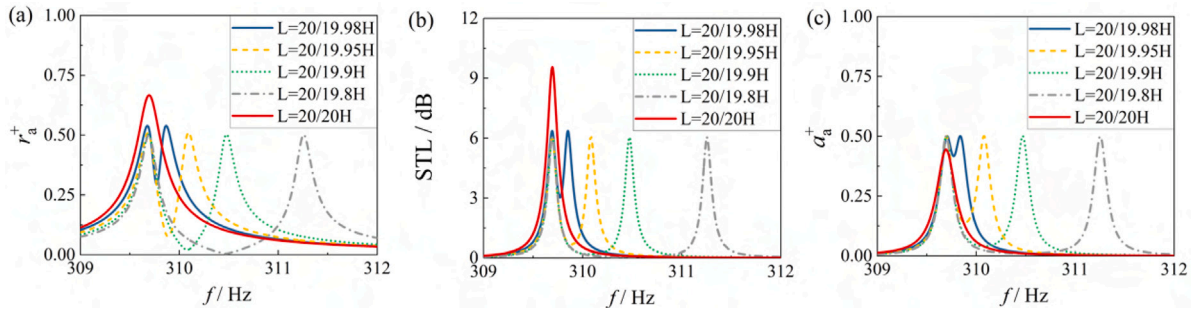


Fig. 9. Influence of bilayer structure with various external inductances L on (a) reflection coefficient, (b) transmission loss, and (c) absorption coefficient in T4 of Table 2.

In the example shown, the incident sound wave is almost totally reflected by the bilayer when the resistance is set to 0.1Ω . The bilayer's absorption coefficient goes up to about 0.5 in Fig. 8(c) by optimizing the external resistance. As a result, the external resistance provides a way to control and improve the sound-absorbing or insulating properties of the piezoelectric AM.

Improved acoustic properties and broader bandwidth can be achieved by introducing multi-layer structures made of several piezoelectric AMs. A simple bilayer structure is studied to investigate its acoustic performance. The external inductance is varied between the layers, leading to several combinations of external inductances in the multiple structures, see Fig. 9. For instance, setting the two external inductances at 20 and 19.8 H provides two distinct resonance peaks in this design of AM. But the resonance frequencies can be moved closer and overlapped by reducing the difference between the external inductances. This results in a greater reflection coefficient, and it may be expected that a band gap could be produced with multiple layers. The results illustrate that multiple piezoelectric AM structures can generate various resonance frequencies and broaden or tailor the bandwidth through adjustment of the external components.

4.3. Acoustic performance at low and high frequency

The resonance frequency can be tuned over a wide range by adjusting the external circuit. The resonance depends on the internal capacitance of the piezoelectric layer C_0^S , external capacitance C , and external inductance L . However, the choices of inductance and capacitance in the external circuit are practically limited by available electronic components. Taking typical ranges for readily available inductors and capacitors of $1 \mu\text{H}$ to 20 H [70,71] and 1 mF to 1 pF [72,73], respectively, the acoustic performance of a piezoelectric AM at low and high resonance frequencies can be assessed.

Choosing L and C to provide a constant resonance frequency less than 1 kHz , the low-frequency acoustic performance can be explored by varying external resistance R , see Fig. 10. The peak reflection coefficient rises from about 0.1 to 0.9 when reducing the external resistance from 100 to 0.1Ω , as shown in Fig. 10(a). Meanwhile, the peak in the value of the transmission loss is almost unaffected when R is varied from 0.1 and 1Ω , but increasing the resistance to 100Ω greatly reduce the transmission loss as seen in Fig. 10(b). In general, a low maximum reflection coefficient and a low minimum transmission coefficient lead to a high sound absorption coefficient. The maximum sound absorption coefficient at resonance reaches 0.5 in Fig. 10(c), achieved by setting the resistance as 10Ω , and demonstrating that the external resistance can be used to optimize acoustic performance.

For a piezoelectric layer with a fixed cross-sectional area, the internal capacitance is inversely proportional to the layer thickness. Using a series of practical layer thickness values, from 0.5 to 8 mm , the influence of layer thickness on the acoustic performance is illustrated in Fig. 11. This shows that changing the layer thickness affects both the resonance frequency, the sound reflection coefficient, transmission loss, and absorption coefficient. Generally, a thicker layer reduces transmission and increases bandwidth, but note that the absorption coefficient first rises and then falls with increasing layer thickness. There is a trade-off between the

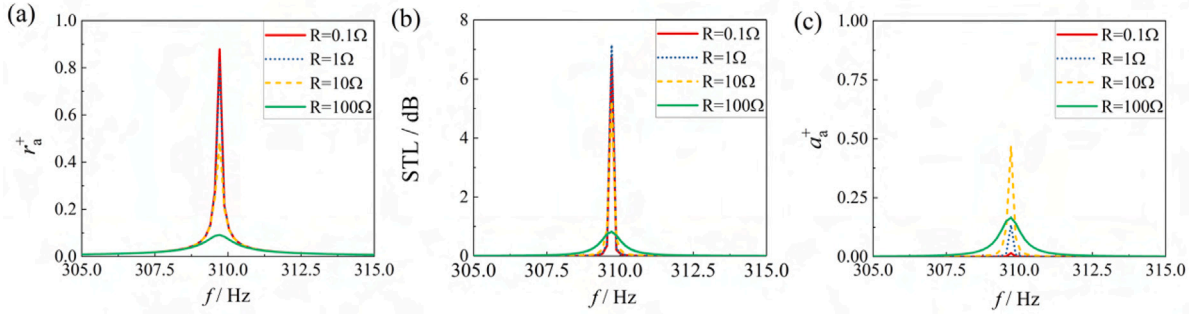


Fig. 10. Influence of external resistance R on (a) reflection coefficient, (b) transmission loss, and (c) absorption coefficient at low-frequency range in T5 of Table 2.

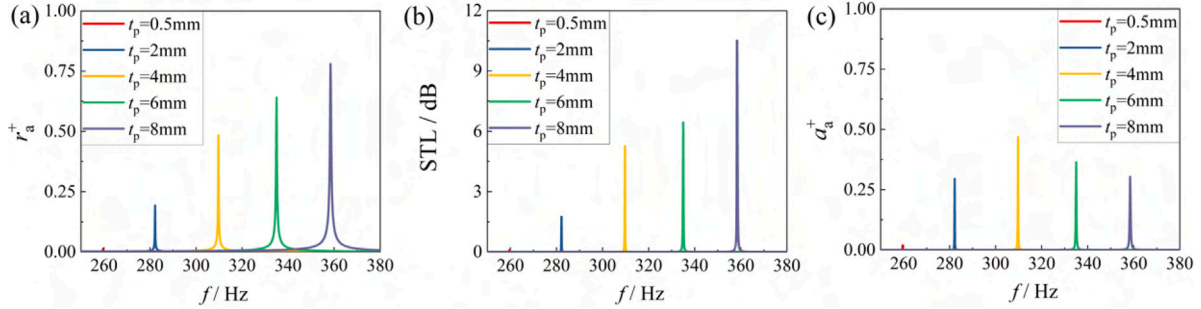


Fig. 11. Influence of PZT-5H layer thickness t_p on (a) reflection coefficient, (b) transmission loss, and (c) absorption coefficient at low-frequency range in T6 of Table 2.

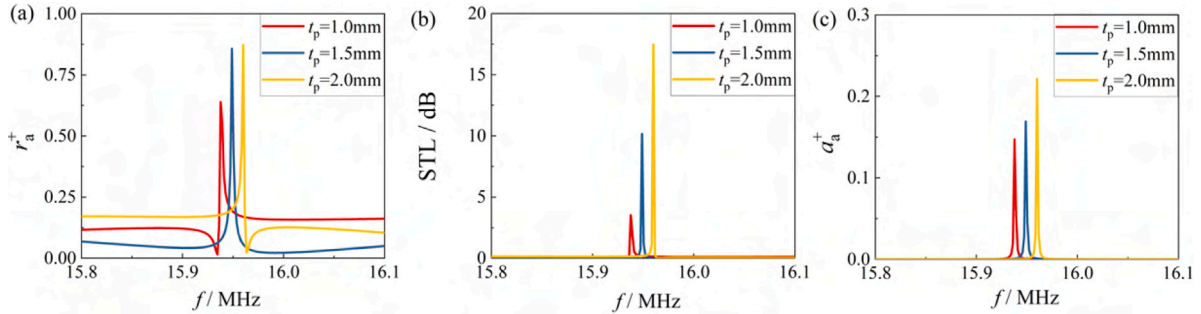


Fig. 12. Influence of PZT-5H layer thickness t_p on (a) reflection coefficient, (b) transmission loss, and (c) absorption coefficient at high-frequency range in T7 of Table 2.

increasing mass of the thicker layer and its reduced capacitance, offering an opportunity to tailor the design, taking account of material costs and practical size limits, but using the external components to tune the performance in service.

The use of a piezoelectric layer in a plate-type AM results in deep sub-wavelength device size. For instance, a 4 mm-thick PZT-5H layer can reflect the incident sound waves or absorb a large percentage of the incident sound energy at a frequency of about 310 Hz, which is about $1/4250$ of the resonance wavelength in steel. This deeply sub-wavelength level, less than 10^{-3} of the resonance wavelength, is far beyond the wavelength-to-thickness ratios of current passive AMs.

Similar trends can be observed at high frequencies in the analytical results of Fig. 12. The resonance frequency increases as the external inductance or capacitance is reduced. The piezoelectric AM works effectively to reflect and absorb incident waves at frequencies up to the MHz range. Increasing the layer thickness from 1 to 2 mm, slightly shifts the resonance frequency but at this operating frequency range the reciprocal of the internal capacitance is about one hundred times smaller than the reciprocal of the external capacitance, so changing the internal capacitance has little effect.

4.4. Optimized acoustic performance at a target frequency

The values of capacitance C , resistance R and inductance L in the external circuit, thickness t_p and cross-sectional area A of the piezoelectric layer (PZT-5H) have simultaneous effects on both acoustic performance and resonance frequency of the piezoelectric

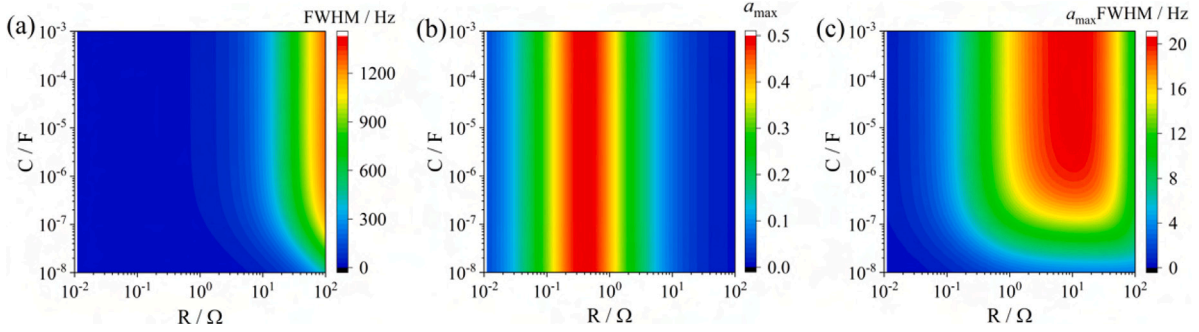


Fig. 13. Influence of resistance R and capacitance C on (a) FWHM, (b) a_{\max} , and (c) $a_{\max} \text{FWHM}$ at the target frequency of 9455 Hz.

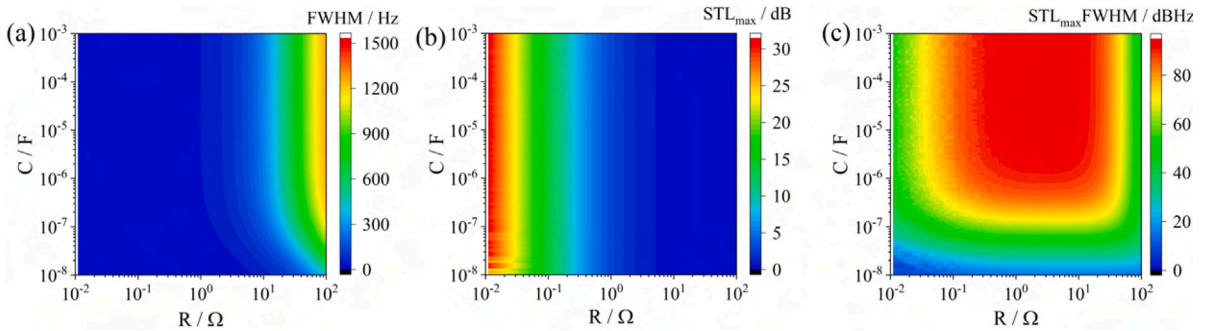


Fig. 14. Influence of resistance R and capacitance C on (a) FWHM, (b) STL_{\max} , and (c) $\text{STL}_{\max} \text{FWHM}$ at a target frequency of 9455 Hz.

AM. The resonance bandwidth reflects the piezoelectric resonator's capability to be coupled with an incident acoustic wave. The sound absorption peak is not the only aspect to evaluate when assessing the acoustic properties; the bandwidth of the resulting peak should also be examined. For this reason, the full width at half maximum FWHM, maximum sound absorption coefficient a_{\max} , maximum sound transmission loss STL_{\max} and their product values, $a_{\max} \text{FWHM}$ and $\text{STL}_{\max} \text{FWHM}$, are used to evaluate overall acoustic performance at a fixed resonance frequency (here 9.455 kHz). The choice of cross-sectional area and thickness of a piezoelectric layer is usually determined by the application and the fabrication process in real applications; here, these have been fixed at $A = 400 \text{ mm}^2$ and $t_p = 0.2 \text{ mm}$ respectively. To optimize acoustic performance at resonance, the external inductance serves as a dependent variable to maintain the resonance frequency constant as other parameters vary. The independent variables are then the resistance, R , and external capacitance, C ; these are varied over a range from 10^{-2} to $10^2 \Omega$ and from 10^{-8} to 10^{-3} F, respectively.

Fig. 13 shows the effect of R and C on the FWHM frequency range of sound absorption, the sound absorption coefficient a_{\max} , and their product. On increasing R over several orders, the FWHM of the sound absorption coefficient increases from a few Hz to more than 1200 Hz, but the sound absorption coefficient is low over most of the range: a_{\max} peaks sharply for R ranging from 10^{-1} to $10^0 \Omega$ but falls away with further increase in R . The sound absorption coefficients are almost independent of the value of C for $C > 10^{-8}$ F. This illustrates the need for an optimized external resistance to obtain maximum sound absorption. The product $a_{\max} \text{FWHM}$ can be used as an overall sound-absorbance metric, see Fig. 13(c). It has a plateau at around 20 Hz for the optimized resistance and capacitance ranging from 10^0 to $10^2 \Omega$ and from 10^{-7} to 10^{-3} F, respectively.

Fig. 14 shows corresponding results for the FWHM of sound transmission loss, STL_{\max} , and their product. The FWHM grows from a few Hz to about 1500 Hz as the resistance rises to $10^2 \Omega$ while the maximum sound transmission loss peaks at around 30 dB when R is below 0.03Ω . The overall sound-insulation metric $\text{STL}_{\max} \text{FWHM}$ plateaus at around 80 dBHz for resistance and capacitance in the range 10^{-1} to $10^2 \Omega$ and 10^{-7} to 10^{-3} F, respectively, before suddenly dropping for larger resistance. Again, the effect of external capacitance is negligible at this target resonance frequency, provided the external capacitance is great enough.

Next, the resistance R and thickness t_p of the piezoelectric AM are set as independent design variables, ranging from 0 to 100Ω and from 0.1 to 40 mm, respectively. The inductance is again used as a dependent variable to fix the resonance frequency at 9.455 kHz. The external capacitance and the cross-sectional area of the piezoelectric PZT-5H layer are held constant at $C = 20 \text{ nF}$ and $A = 400 \text{ mm}^2$, respectively.

Fig. 15 shows that the FWHM of the sound absorption coefficient of the piezoelectric AM gradually climbs with increasing t_p , almost independent of R . Meanwhile, the maximum sound absorption coefficient peaks at about 0.5 for layers thinner than 5 mm, the optimum R varying with layer thickness. However, for thicker piezoelectric layers, the maximum sound absorption coefficient is small for the range of resistance considered. As a result, the product $a_{\max} \text{FWHM}$ peaks at the top of the resistance range and with

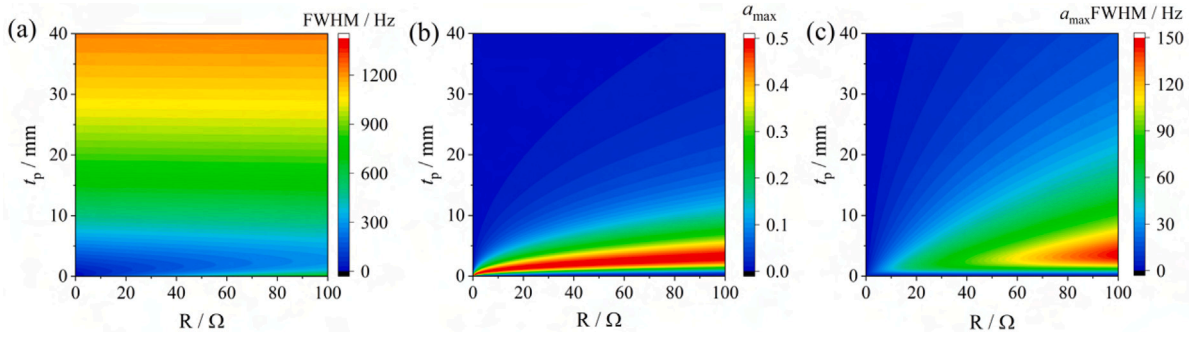


Fig. 15. Influence of resistance R and PZT-5H thickness t_p on (a) FWHM, (b) a_{\max} , and (c) a_{\max} FWHM at the target frequency of 9455 Hz.

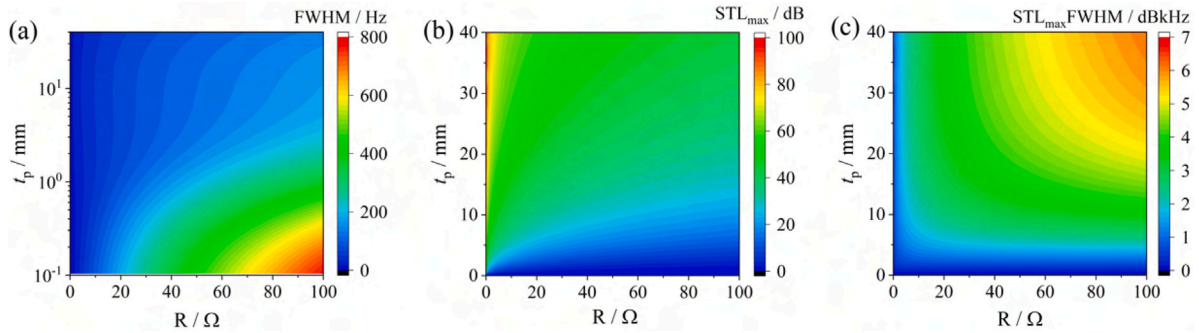


Fig. 16. Influence of resistance R and PZT-5H thickness t_p on (a) FWHM, (b) STL_{\max} , and (c) STL_{\max} FWHM at the target frequency of 9455 Hz.

a specific t_p value, in this example around 4 mm. In other words, greater thicknesses and smaller resistances result in poor overall sound-absorbing performance near the resonance.

Corresponding results for sound transmission loss in Fig. 16 show an interesting compromise: FWHM is greatest for thin layers at high shunt resistance, but the STL_{\max} would be optimized at low values of R below 5 Ω and a thick layer. If the maximum of the product STL_{\max} FWHM is sought, it is instead achieved by combining high R values with high layer thickness. This last example illustrates the trade-off between different objectives for acoustic isolation. The optimum design and configuration is strongly dependent on what aspect of the performance is most significant, and this may vary with application.

4.5. Summary

In summary, the resonance frequency of the piezoelectric AM can be tuned effectively through an external circuit to control incident longitudinal sound waves in steel. The acoustic performance is readily tunable over a vast frequency range from hundreds of Hz to up to MHz, by adjusting the inductance and capacitance in the external circuit rather than having to modify the AM's structure and thickness. Besides, the piezoelectric AM's acoustic performance at a resonance frequency can be optimized by controlling the resistance in the external circuit.

In addition, the thickness of the piezoelectric AM can reach a deep sub-wavelength size far beyond the limits of membrane and Helmholtz resonator types of AM; typical sizes are less than 1/1000 of the resonant wavelength in steel. The AM can form an effective reflector or absorber of incident sound waves, under the control of the external electrical impedance. This breaks the general normal incidence mass law and shows excellent performance in resonance frequency tunability.

Detailed optimization of the FWHM, a_{\max} , STL_{\max} , and their product values, illustrates that design compromises must be made, and that careful selection of parameter values is needed to achieve effective control of sound waves.

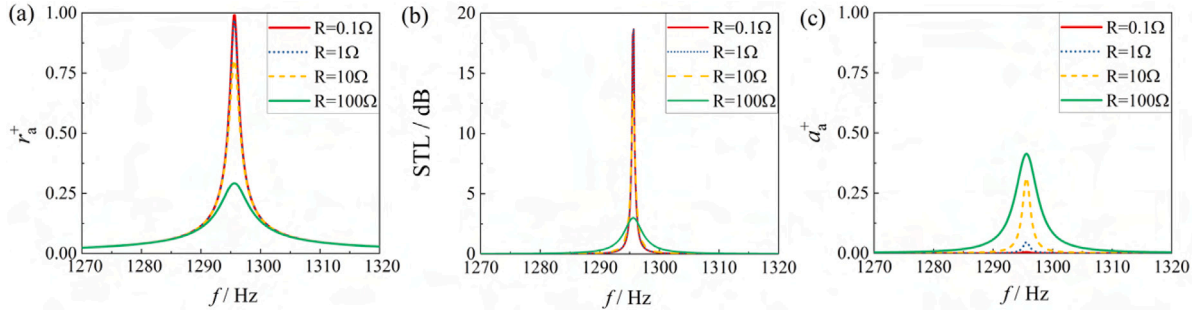
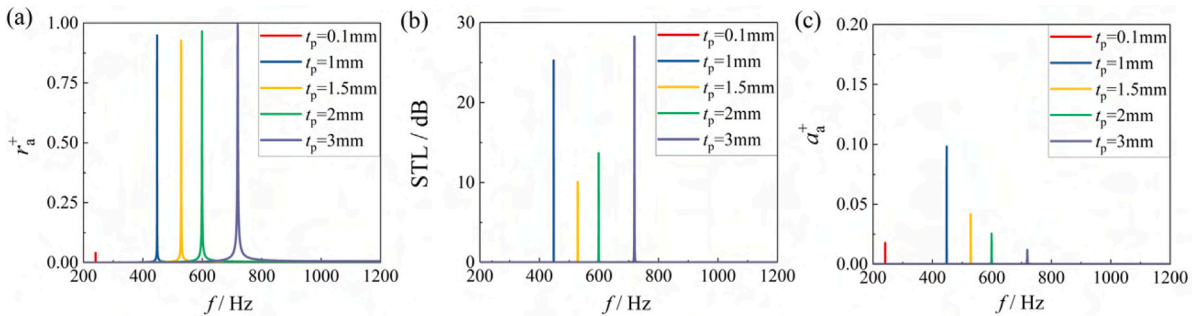
5. Acoustic performance of piezoelectric AMs in water and air

Noting the wide variety of media in which sound suppression may be needed, this section explores the performance of a piezoelectric layered AM in two media with greatly differing densities, elastic moduli and wave speeds: water and air. In water, piezoelectric polyvinylidene difluoride (PVDF) is adopted as the active layer, providing a better impedance match to water compared with PZT-5H materials. The relevant properties of water and PVDF are given in Table 1.

First, the AM performance at low (audible) frequencies is considered, using parameters that place the resonance frequency close to 1.3 kHz. The effects of external resistance on sound reflection coefficient, transmission loss and absorption coefficient are studied

Table 3Acoustic performance tests in water and air using a single piezoelectric layer (\times : variables).

Component	Property	T8	T9	T10	T11	T12	T13
Medium		Water	Water	Water	Air	Air	Air
Piezo materials		PVDF	PVDF	PVDF	PZT-5H	PVDF	fibrous PVDF
Structure	t_p /mm	1	\times	\times	1	1	1
	A /m ²	0.04	0.09	0.09	0.01	0.01	0.01
Circuit	C /nF	20	30	20	20	20	20
	L /mH	5k	20k	0.27	20	20	20
	R / Ω	\times	1	0.1	1	1	1

**Fig. 17.** Influence of external resistance R on (a) reflection coefficient, (b) transmission loss, and (c) absorption coefficient in water at low-frequency range in T8 of Table 3.**Fig. 18.** Influence of PVDF membrane thickness t_p on (a) reflection coefficient, (b) transmission loss, and (c) absorption coefficient in water at low-frequency range in T9 of Table 3.

with R varying from 10^{-1} to $10^2 \Omega$, see Fig. 17. At resonance, the reflection coefficient peaks close to unity for low R values; the peak reflection coefficient then reduces as R is increased beyond 1Ω . The transmission loss shows a similar trend, while the absorption coefficients and their corresponding bandwidths witness a gradual increase with resistance. Thus the reflection and absorption can again be controlled through the selection of the external resistance.

Variation of the layer thickness in the low-frequency configuration is studied in Fig. 18. Reducing the PVDF layer thickness also reduces the resonance frequency, and the reflection coefficient drops sharply for layer thickness less than 1 mm. The sound absorption coefficient remains less than 0.1 for all the thickness values shown. The zero-width peak shows that the coupling between the incident sound wave and the PVDF film is weak, resulting in poor sound absorption. The piezoelectric AM with a 1 mm thick PVDF membrane works efficiently as a sound reflector at frequencies around 450 Hz, at which point, the piezoelectric AM size is less than $1/3000$ of the target resonance wavelength, illustrating the deep sub-wavelength capabilities of the piezoelectric layered AM.

Next, consider the high-frequency performance of this AM in water. By reducing the external inductance to about 0.27 mH, resonant frequencies of the order of 100 kHz are accessed. The effect of varying the PVDF layer thickness t_p from 0.1 to 0.9 mm is illustrated in Fig. 19. As t_p increases, the resonance bandwidth increases, while the peak reflection coefficient rises to near unity (total reflection), and there is a corresponding increase in the transmission loss. The sound absorption coefficient experiences a considerable drop from 0.45 to 0.02, see Fig. 19(c). The piezoelectric AM with a PVDF layer can work as an excellent high-frequency sound barrier with a tunable frequency exceeding 100 kHz in water. Combined with the low-frequency performance, this suggests that layered piezoelectric AMs can manipulate longitudinal waves over a frequency range covering most practical applications in water [74].

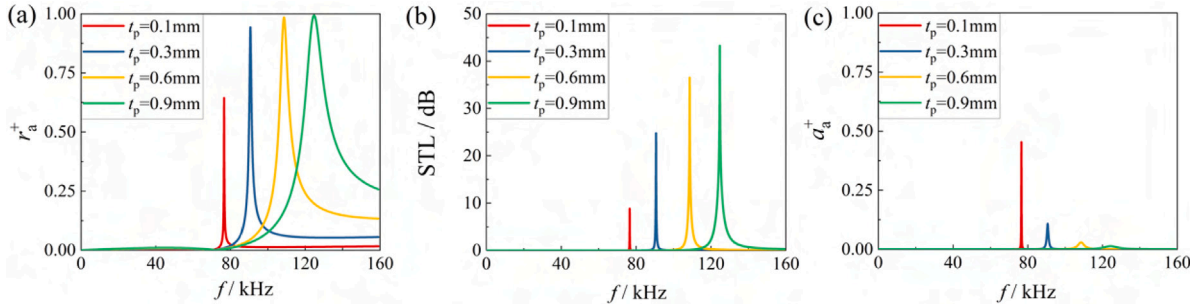


Fig. 19. Influence of PVDF membrane thickness t_p on (a) reflection coefficient, (b) transmission loss, and (c) absorption coefficient in water at high-frequency range in T10 of Table 3.

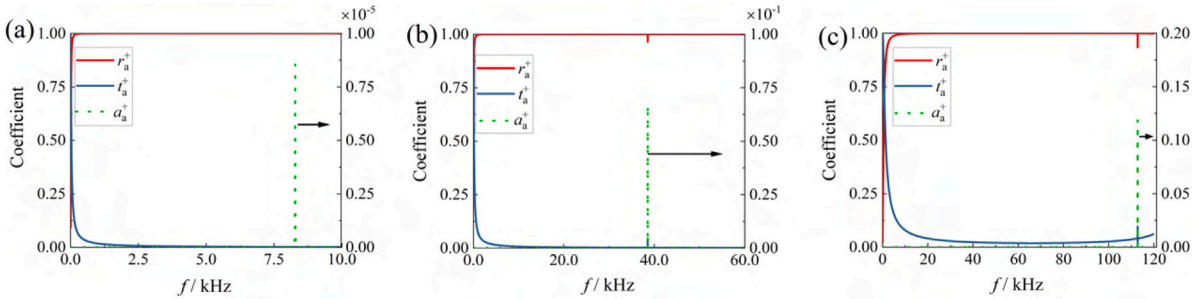


Fig. 20. Acoustic performance of various piezoelectric materials including (a) PZT-5H, (b) PVDF, and (c) fibrous PVDF in air.

Finally, a range of piezoelectric materials, including PZT-5H, PVDF, and fibrous PVDF, are considered as candidates for the active layer in a piezoelectric layered AM for operation in air. The relevant material properties are listed in Table 1. Fibrous PVDF membranes can be fabricated by electrospinning technology or 3D printing technology. However, analytical prediction of the properties of such fibrous membranes is challenging; the estimated values used here were obtained from [59–65]. The external circuit parameters and thickness of piezoelectric layers are held constant, while the choice of active material is varied as indicated in Table 3. Controlling acoustic waves in air using solid layers is challenging because of the extreme mismatch in acoustic impedance between the air and the solid layers. Thus the solid layer tends to have a resonance effect only at a very sharply defined frequency and behaves more like a passive layer away from the resonance frequency. There is relatively little ability to absorb sound, though reflection coefficients tend to be high.

The acoustic performance of the PZT-5H layered AM is reported in Fig. 20(a). The resonance frequency for this configuration is about 8 kHz but note the almost negligible sound absorption coefficient: this system strongly reflects incident sound energy because of the acoustic impedance mismatch between air and PZT-5H. A similar result is seen with the PVDF layer in Fig. 20(b). Using a fibrous PVDF membrane as the active element greatly reduces the impedance mismatch and provides high dielectric permittivity; the material properties may be controlled through the PVDF fibre diameter and porosity, enabling acoustic matching while maintaining attractive electrical performance [75–77]. As a result, the sound absorption coefficient reaches about 0.12 at the resonance frequency, see Fig. 20(c). This indicates an excellent potential to absorb sound at a controllable frequency in air, using a much thinner sound linear structure than is possible with conventional approaches.

6. Conclusion

The acoustic performance of piezoelectric AMs, in the form of a piezoelectric layer with an external electrical impedance, was studied analytically through the transfer matrix method and numerically using the finite element method for normal incident sound waves. For the first time, these findings are also validated using experimental data. The performance of various shunted piezoelectric materials, including PZT-5H, PVDF and fibrous PVDF foams, in a range of media, was investigated. The results indicate that the acoustic performance, such as sound reflection coefficient, transmission loss and absorption coefficient, can be manipulated by adjusting external circuit resistance, while the resonance frequency of the piezoelectric AM can be tuned through the external inductance and capacitance. This endows the AM with a highly versatile acoustic response through a conceptually simple mechanism.

Calculations demonstrate that the piezoelectric AM's size can be deeply subwavelength while still offering effective and controllable wave manipulation. Control of key metrics such as device bandwidth, sound absorption and sound transmission loss can be achieved over a wide range of values by modifying external impedance alone. However, trade-offs were observed between these metrics, indicating a need for careful selection of electrical parameters in practical applications. Varying the external medium from

steel to water or to air required a change in piezoelectric material and layer thickness in order to achieve effective wave control, due to impedance mismatch. By introducing fibrous PVDF membranes with greatly reduced acoustic impedance relative to other piezoelectrics, effective noise reduction in air was predicted.

Overall, layered piezoelectric AMs are found to offer a relatively simple, versatile and tunable form of wave control for normally incident plane waves. Further work is needed to assess the performance of these AMs for more challenging wave manipulation tasks, but the results here indicate great potential for these systems for noise reduction, which is in high demand in space-sensitive applications.

Declaration of competing interest

The authors declare that they have no known competing financial interests or personal relationships that could have appeared to influence the work reported in this paper.

Data availability

Data will be made available on request.

Acknowledgements

Guosheng Ji is supported by the Clarendon Fund and Trinity College Scholarship at the University of Oxford. Dr. Zhou is grateful for the financial support from the National Natural Science Foundation of China (GrantNo. 12072277).

Appendix A. Supplementary data

Supplementary material related to this article can be found online at <https://doi.org/10.1016/j.ymssp.2023.110549>.

References

- [1] F.J. Fahy, *Foundations of Engineering Acoustics*, Elsevier, 2000.
- [2] R. Kim, et al., Burden of disease from environmental noise, in: WHO International Workshop on “Combined Environmental Exposure: Noise, Air Pollutants and Chemicals” Ispra, 2007.
- [3] F.J. Fahy, P. Gardonio, *Sound and Structural Vibration: Radiation, Transmission and Response*, Elsevier, 2007.
- [4] T.J. Cui, D.R. Smith, R. Liu, *Metamaterials*, Springer, 2010.
- [5] G. Ma, *Membrane-type acoustic metamaterials* (Ph.D. thesis), Hong Kong University of Science and Technology, 2012.
- [6] F. Ma, M. Huang, J.H. Wu, Ultrathin lightweight plate-type acoustic metamaterials with positive lumped coupling resonant, *J. Appl. Phys.* 121 (1) (2017) 015102.
- [7] S.A. Cummer, J. Christensen, A. Alù, Controlling sound with acoustic metamaterials, *Nat. Rev. Mater.* 1 (3) (2016) 1–13.
- [8] G. Ji, J. Huber, Recent progress in acoustic metamaterials and active piezoelectric acoustic metamaterials-A review, *Appl. Mater. Today* (2021) 101260.
- [9] G. Ma, P. Sheng, Acoustic metamaterials: From local resonances to broad horizons, *Sci. Adv.* 2 (2) (2016) e1501595.
- [10] M. Yang, P. Sheng, Sound absorption structures: From porous media to acoustic metamaterials, *Annu. Rev. Mater. Res.* 47 (2017) 83–114.
- [11] W. Kang, J.E. Huber, Energy harvesting based on compressive stress-induced ferroelectric/ferroelastic switching in polycrystalline ferroelectric materials, *Cell Rep. Phys. Sci.* 3 (1) (2022) 100707.
- [12] W. Kang, L. Chang, J. Huber, Investigation of mechanical energy harvesting cycles using ferroelectric/ferroelastic switching, *Nano Energy* 93 (2022) 106862.
- [13] W. Sun, G. Ji, J. Chen, D. Sui, J. Zhou, J. Huber, Enhancing the acoustic-to-electrical conversion efficiency of nanofibrous membrane-based triboelectric nanogenerators by nanocomposite composition, *Nano Energy* (2023) 108248.
- [14] J.-P. Groby, C. Lagarrigue, B. Brouard, O. Dazel, V. Tournat, B. Nennig, Enhancing the absorption properties of acoustic porous plates by periodically embedding Helmholtz resonators, *J. Acoust. Soc. Am.* 137 (1) (2015) 273–280.
- [15] X.-F. Zhu, S.-K. Lau, Z. Lu, W. Jeon, Broadband low-frequency sound absorption by periodic metamaterial resonators embedded in a porous layer, *J. Sound Vib.* 461 (2019) 114922.
- [16] G. Ji, Y. Fang, J. Zhou, X. Huang, Porous labyrinthine acoustic metamaterials with high transmission loss property, *J. Appl. Phys.* 125 (21) (2019) 215110.
- [17] T. Yamamoto, Acoustic metamaterial plate embedded with Helmholtz resonators for extraordinary sound transmission loss, *J. Appl. Phys.* 123 (21) (2018) 215110.
- [18] M. Duan, C. Yu, Z. Xu, F. Xin, T.J. Lu, Acoustic impedance regulation of Helmholtz resonators for perfect sound absorption via roughened embedded necks, *Appl. Phys. Lett.* 117 (15) (2020) 151904.
- [19] G. Ji, Y. Fang, J. Zhou, Porous acoustic metamaterials in an inverted wedge shape, *Extreme Mech. Lett.* 36 (2020) 100648.
- [20] G. Ji, J. Xu, J. Zhou, W. Kang, The exploration of transmission property by using the circular-interface types of porous acoustic metamaterials, *Int. J. Mech. Sci.* (2022) 107558.
- [21] N. Jiménez, T.J. Cox, V. Romero-García, J.-P. Groby, Metadiffusers: Deep-subwavelength sound diffusers, *Sci. Rep.* 7 (1) (2017) 1–12.
- [22] X. Chen, P. Liu, Z. Hou, Y. Pei, Magnetic-control multifunctional acoustic metasurface for reflected wave manipulation at deep subwavelength scale, *Sci. Rep.* 7 (1) (2017) 1–9.
- [23] J. Chen, J. Xiao, D. Lisevych, A. Shakouri, Z. Fan, Deep-subwavelength control of acoustic waves in an ultra-compact metasurface lens, *Nature Commun.* 9 (1) (2018) 1–9.
- [24] Y. Wang, H. Zhao, H. Yang, J. Zhong, D. Zhao, Z. Lu, J. Wen, A tunable sound-absorbing metamaterial based on coiled-up space, *J. Appl. Phys.* 123 (18) (2018) 185109.
- [25] M. Boccaccio, F. Bucciarelli, G.P.M. Fierro, M. Meo, Microperforated panel and deep subwavelength archimedean-inspired spiral cavities for multi-tonal and broadband sound absorption, *Appl. Acoust.* 176 (2021) 107901.
- [26] X. Zhu, J. Qiao, G. Shao, G. Zhang, L. Li, A tunable acoustic metamaterial based on piezo buzzers and passive circuits, *Appl. Phys. Express* 12 (12) (2019) 127002.

- [27] M. Danesh, A. Ghadami, Sound transmission loss of double-wall piezoelectric plate made of functionally graded materials via third-order shear deformation theory, *Compos. Struct.* 219 (2019) 17–30.
- [28] Z. Hou, B.M. Assouar, Tunable solid acoustic metamaterial with negative elastic modulus, *Appl. Phys. Lett.* 106 (25) (2015) 251901.
- [29] Z. Hou, B. Assouar, Tunable elastic parity-time symmetric structure based on the shunted piezoelectric materials, *J. Appl. Phys.* 123 (8) (2018) 085101.
- [30] S.-W. Fan, S.-D. Zhao, A.-L. Chen, Y.-F. Wang, B. Assouar, Y.-S. Wang, Tunable broadband reflective acoustic metasurface, *Phys. Rev. A* 11 (4) (2019) 044038.
- [31] P. Wang, F. Casadei, S. Shan, J.C. Weaver, K. Bertoldi, Harnessing buckling to design tunable locally resonant acoustic metamaterials, *Phys. Rev. Lett.* 113 (1) (2014) 014301.
- [32] Z. Tian, C. Shen, J. Li, E. Reit, Y. Gu, H. Fu, S.A. Cummer, T.J. Huang, Programmable acoustic metasurfaces, *Adv. Funct. Mater.* 29 (13) (2019) 1808489.
- [33] B. Xia, N. Chen, L. Xie, Y. Qin, D. Yu, Temperature-controlled tunable acoustic metamaterial with active band gap and negative bulk modulus, *Appl. Acoust.* 112 (2016) 1–9.
- [34] S. Ning, Z. Yan, D. Chu, H. Jiang, Z. Liu, Z. Zhuang, Ultralow-frequency tunable acoustic metamaterials through tuning gauge pressure and gas temperature, *Extreme Mech. Lett.* 44 (2021) 101218.
- [35] R.L. Forward, Electronic damping of vibrations in optical structures, *Appl. Opt.* 18 (5) (1979) 690–697.
- [36] N.W. Hagood, A. von Flotow, Damping of structural vibrations with piezoelectric materials and passive electrical networks, *J. Sound Vib.* 146 (2) (1991) 243–268.
- [37] B.S. Beck, K.A. Cunefare, M. Ruzzene, M. Collet, Experimental analysis of a cantilever beam with a shunted piezoelectric periodic array, in: *Smart Materials, Adaptive Structures and Intelligent Systems*, Vol. 44151, 2010, pp. 565–573.
- [38] F. Tateo, M. Collet, M. Ouisse, M. Ichchou, K. Cunefare, P. Abbé, Experimental characterization of a bi-dimensional array of negative capacitance piezo-patches for vibroacoustic control, *J. Intell. Mater. Syst. Struct.* 26 (8) (2015) 952–964.
- [39] J. Kim, J.-k. Lee, Broadband transmission noise reduction of smart panels featuring piezoelectric shunt circuits and sound-absorbing material, *J. Acoust. Soc. Am.* 112 (3) (2002) 990–998.
- [40] S. Chen, G. Wang, J. Wen, X. Wen, Wave propagation and attenuation in plates with periodic arrays of shunted piezo-patches, *J. Sound Vib.* 332 (6) (2013) 1520–1532.
- [41] T. Ma, Y. Chen, H. Chen, Y. Zheng, G. Huang, J. Wang, J. Du, Tuning characteristics of a metamaterial beam with lateral-electric-field piezoelectric shuntings, *J. Sound Vib.* 491 (2021) 115738.
- [42] F. Casadei, T. Delpero, A. Bergamini, P. Ermanni, M. Ruzzene, Piezoelectric resonator arrays for tunable acoustic waveguides and metamaterials, *J. Appl. Phys.* 112 (6) (2012) 064902.
- [43] Y. Chen, G. Hu, G. Huang, An adaptive metamaterial beam with hybrid shunting circuits for extremely broadband control of flexural waves, *Smart Mater. Struct.* 25 (10) (2016) 105036.
- [44] L. Airolidi, M. Ruzzene, Design of tunable acoustic metamaterials through periodic arrays of resonant shunted piezos, *New J. Phys.* 13 (11) (2011) 113010.
- [45] Y. Chen, R. Zhu, M.V. Barnhart, G. Huang, Enhanced flexural wave sensing by adaptive gradient-index metamaterials, *Sci. Rep.* 6 (1) (2016) 1–11.
- [46] Y. Chen, G. Hu, G. Huang, A hybrid elastic metamaterial with negative mass density and tunable bending stiffness, *J. Mech. Phys. Solids* 105 (2017) 179–198.
- [47] X. Li, Y. Chen, R. Zhu, G. Huang, An active meta-layer for optimal flexural wave absorption and cloaking, *Mech. Syst. Signal Process.* 149 (2021) 107324.
- [48] O. Thorp, M. Ruzzene, A. Baz, Attenuation and localization of wave propagation in rods with periodic shunted piezoelectric patches, *Smart Mater. Struct.* 10 (5) (2001) 979.
- [49] E.A. Flores Parra, A. Bergamini, B. Lossouarn, B. Van Damme, M. Cenedese, P. Ermanni, Bandgap control with local and interconnected LC piezoelectric shunts, *Appl. Phys. Lett.* 111 (11) (2017) 111902.
- [50] C. Sugino, M. Ruzzene, A. Erturk, An analytical framework for locally resonant piezoelectric metamaterial plates, *Int. J. Solids Struct.* 182 (2020) 281–294.
- [51] C. Sugino, M. Ruzzene, A. Erturk, Design and analysis of piezoelectric metamaterial beams with synthetic impedance shunt circuits, *IEEE/ASME Trans. Mechatronics* 23 (5) (2018) 2144–2155.
- [52] L. Airolidi, M. Ruzzene, Wave propagation control in beams through periodic multi-branch shunts, *J. Intell. Mater. Syst. Struct.* 22 (14) (2011) 1567–1579.
- [53] A. Erturk, D.J. Inman, A distributed parameter electromechanical model for cantilevered piezoelectric energy harvesters, *J. Vib. Acoust.* 130 (4) (2008).
- [54] A. Spadoni, M. Ruzzene, K. Cunefare, Vibration and wave propagation control of plates with periodic arrays of shunted piezoelectric patches, *J. Intell. Mater. Syst. Struct.* 20 (8) (2009) 979–990.
- [55] F. Casadei, M. Ruzzene, L. Dozio, K. Cunefare, Broadband vibration control through periodic arrays of resonant shunts: experimental investigation on plates, *Smart Mater. Struct.* 19 (1) (2009) 015002.
- [56] J. Allard, N. Atalla, *Propagation of Sound in Porous Media: Modelling Sound Absorbing Materials 2e*, John Wiley & Sons, 2009.
- [57] T. Cox, P. D'Antonio, *Acoustic Absorbers and Diffusers: Theory, Design and Application*, CRC Press, 2016.
- [58] R.A. Reyes-Villagrana, G. Gutiérrez-Juárez, R. Ivanov-Tzontchev, Characterization of simulated mechanical-electrical properties of PVDF and PZT piezoelectric material for use in the pulsed optoacoustic spectroscopy, *IJPAST*, (2) (2011) 26–45.
- [59] M.F. Ashby, R.M. Medalist, The mechanical properties of cellular solids, *Metall. Trans. A* 14 (9) (1983) 1755–1769.
- [60] M.F. Ashby, The properties of foams and lattices, *Phil. Trans. R. Soc. A* 364 (1838) (2006) 15–30.
- [61] G. Ji, J. Cui, Y. Fang, S. Yao, J. Zhou, J.-K. Kim, Nano-fibrous composite sound absorbers inspired by owl feather surfaces, *Appl. Acoust.* 156 (2019) 151–157.
- [62] K. Rittenmyer, T. Shrout, W. Schulze, R. Newnham, Piezoelectric 3–3 composites, *Ferroelectrics* 41 (1) (1982) 189–195.
- [63] Z. Yong, et al., Research on structure-property relationships of micro-architected metamaterials (Ph.D. thesis), Hong Kong Polytechnic University, 2018.
- [64] H. Cui, R. Hensleigh, D. Yao, D. Maurya, P. Kumar, M.G. Kang, S. Priya, X.R. Zheng, Three-dimensional printing of piezoelectric materials with designed anisotropy and directional response, *Nature Mater.* 18 (3) (2019) 234–241.
- [65] E.F. Knott, Dielectric constant of plastic foams, *IEEE Trans. Antennas and Propagation* 41 (8) (1993) 1167–1171.
- [66] B.-I. Popa, D. Shinde, A. Konneker, S.A. Cummer, Active acoustic metamaterials reconfigurable in real time, *Phys. Rev. B* 91 (22) (2015) 220303.
- [67] Y. Li, B. Liang, Z.-m. Gu, X.-y. Zou, J.-c. Cheng, Reflected wavefront manipulation based on ultrathin planar acoustic metasurfaces, *Sci. Rep.* 3 (1) (2013) 1–6.
- [68] H. Chang, L. Liu, C. Zhang, X. Hu, Broadband high sound absorption from labyrinthine metasurfaces, *AIP Adv.* 8 (4) (2018) 045115.
- [69] Z. Liu, X. Zhang, Y. Mao, Y. Zhu, Z. Yang, C.T. Chan, P. Sheng, Locally resonant sonic materials, *Science* 289 (5485) (2000) 1734–1736.
- [70] L. Marchetti, A. Romi, Y. Berg, O. Mirmotahari, M. Azadmehr, A discrete implementation of a bidirectional circuit for actuation and read-out of resonating sensors, in: *2016 International Conference on Design and Technology of Integrated Systems in Nanoscale Era, DTIS, IEEE*, 2016, pp. 1–5.
- [71] J. Tao, X. Yu, Influence of shunt-damping circuit on the dynamic response of a bio-inspired piezoelectric micropillar sensor, in: *Bioinspiration, Biomimetics, and Bioreplication 2014*, Vol. 9055, International Society for Optics and Photonics, 2014, p. 90550J.
- [72] V.S. Kumar, P.K. Gupta, L. Hiremath, S.N. Kumar, A.K. Srivastava, A trend in future bioenergy-A review, *J. Pharm. Res.* 12 (2) (2018) 200.
- [73] P. Chacko, K. Kapildas, et al., Nano generator intended for energy harvesting, *Asian J. Appl. Sci. Technol. (AJAST)* 1 (9) (2017) 88–91.
- [74] C. Audoly, Acoustic metamaterials and underwater acoustics applications, in: *Fundamentals and Applications of Acoustic Metamaterials: From Seismic to Radio Frequency*, Vol. 1, Wiley Online Library, 2019, pp. 263–285.

- [75] C. Perrot, F. Chevillotte, R. Panneton, Bottom-up approach for microstructure optimization of sound absorbing materials, *J. Acoust. Soc. Am.* 124 (2) (2008) 940–948.
- [76] S. Liu, W. Chen, Y. Zhang, Design optimization of porous fibrous material for maximizing absorption of sounds under set frequency bands, *Appl. Acoust.* 76 (2014) 319–328.
- [77] C. Perrot, F. Chevillotte, R. Panneton, Dynamic viscous permeability of an open-cell aluminum foam: Computations versus experiments, *J. Appl. Phys.* 103 (2) (2008) 024909.